

PAPER • OPEN ACCESS

## Flat optics in high numerical aperture broadband imaging systems

To cite this article: Daniel Werdehausen *et al* 2020 *J. Opt.* **22** 065607

View the [article online](#) for updates and enhancements.

You may also like

- [Diffractive optics for axial intensity shaping of Bessel beams](#)  
Raghu Dharmavarapu, Shanti Bhattacharya and Saulius Juodkazis
- [DMD maskless digital lithography based on stepwise rotary stitching](#)  
Qixiang Yuan, Chunxia Liu, Long Huang et al.
- [Simple and universal method in designs of high-efficiency diffractive optical elements for spectrum separation and beam concentration](#)  
Wen-Qi Xu, , Dong-Feng Lin et al.

# Flat optics in high numerical aperture broadband imaging systems

Daniel Werdehausen<sup>1,2</sup> , Sven Burger<sup>3,4</sup>, Isabelle Staude<sup>2</sup> , Thomas Pertsch<sup>2,5</sup> and Manuel Decker<sup>1</sup>

<sup>1</sup> Corporate Research and Technology, Carl Zeiss AG, Carl Zeiss Promenade 10, 07745, Jena, Germany

<sup>2</sup> Institute of Applied Physics, Abbe Center of Photonics, Friedrich Schiller University Jena, Albert-Einstein-Str. 15, 07745, Jena, Germany

<sup>3</sup> JCMwave GmbH, Bolivarallee 22, 14050, Berlin, Germany

<sup>4</sup> Zuse Institute Berlin, Takustr. 7, 14195, Berlin, Germany

<sup>5</sup> Fraunhofer Institute for Applied Optics and Precision Engineering, Albert-Einstein-Str. 7, 07745, Jena, Germany

E-mail: [daniel.werdehausen@zeiss.com](mailto:daniel.werdehausen@zeiss.com)

Received 5 March 2020, revised 17 April 2020

Accepted for publication 29 April 2020

Published 27 May 2020



CrossMark

## Abstract

Diffractive optical elements (DOEs) remain highly underutilized in broadband optical systems even though different technologies for DOEs including échelette-type gratings (EGs), multilevel DOEs, and metagratings have been introduced. Specifically, nanocomposite-enabled EGs can achieve efficiencies of close to 100% throughout the visible spectrum, but only for relatively small diffraction angles. Therefore, the question remains if they are suitable for high-numerical-aperture (NA) systems. Here we show that this is indeed the case. To this end, we first demonstrate that macroscopic nanocomposite-enabled diffractive lenses (DLs) can achieve perfect broadband focusing up to a NA of 0.03. We then derive analytic relationships and investigate prototypical optical designs to show that this threshold fully covers the requirements of high-end imaging systems with  $NA \geq 1$ . This holistic all-system analysis demonstrates that the individual NA of a DL in a broadband imaging system is one to two orders of magnitude lower than the overall system's NA. This shows that high-NA flat optical elements are not required for high-NA broadband systems. Therefore, nanocomposite-enabled EGs can unlock the full potential of DOEs for broadband optical systems, whereas other technologies cannot fulfill their high efficiency requirements.

Keywords: nanocomposites, diffractive optics, optical systems, stray light, propagation, optical design, diffractive optical elements

(Some figures may appear in colour only in the online journal)

## 1. Introduction

Diffractive optical elements (DOEs) have the potential to decrease the size or enhance the performance of a wide range of optical systems [1–8]. For broadband systems, this is mostly

because the anomalous chromatic properties of DOEs make them perfectly suited for correcting chromatic aberrations [2]. In contrast to refractive elements, which rely on curved surfaces to redirect the incident light, DOEs are thin and flat elements ('flat optics') that act on an incident beam of light by locally changing its phase or amplitude as a function of the position. This definition shows that the term DOE encompasses a wide range of devices from conventional échelette-type gratings (EGs) [4, 9, 10], multilevel DOEs [11–14], and holograms [10, 15] to metagratings and metalenses [16–25]. However, despite the considerable research effort into



Original content from this work may be used under the terms of the [Creative Commons Attribution 4.0 licence](https://creativecommons.org/licenses/by/4.0/). Any further distribution of this work must maintain attribution to the author(s) and the title of the work, journal citation and DOI.

these different technologies for DOEs, the widespread use of DOEs in broadband imaging systems has so far mostly remained elusive with only a few exceptions (e.g. [4]). One of the main reasons for this gulf between research and practice is that the diffraction efficiency, which we here define as the power propagating in the desired diffraction order over the total transmitted power, depends on the wavelength, the angle of incidence (AOI), and the grating period [20, 26]. In fact, the technology of multi-layer EGs, which has already been employed in a commercial camera lens [4], only maintains high efficiencies for a narrow range of AOIs [26]. This limitation either imposes severe constraints in the design process or leads to stray light and consequently a general loss of contrast, colorful flares, and ghost images [27–29]. Recently, we have shown that dispersion-engineered nanocomposites in the unrestricted effective medium regime [30–32] allow for the design of EGs which maintain unprecedented high efficiencies across the entire visible spectral range, as well as a wide range of AOIs and grating periods [26, 33, 34]. However, these nanocomposite-enabled EGs only maintain high efficiencies for relatively large grating periods ( $\Lambda > 20 \mu\text{m}$ ). Since large grating periods correspond to small diffraction angles, this raises the question whether they are suitable for high-numerical-aperture (high-NA) broadband systems. Furthermore, the requirements on DLs in real-world optical systems, which must consist of multiple elements to balance all monochromatic and chromatic aberrations [35, 36], have never been comprehensively investigated. In this context, the key question is not whether a high-NA singlet can be realized, but rather if the device is suitable for an overall high-NA system without imposing severe constraints on the system's design or impairing its performance. Such an analysis is urgently required to answer the question of which technology is best suited for unlocking the full potential of DOEs and hence guide the way to a next generation of optical systems.

To analyze the requirements on DLs in high-NA broadband systems and show that nanocomposite-enabled DLs are suitable for such systems, we here present a holistic all-system analysis that accounts for both the microscopic properties of the DLs as well as the requirements of the overall systems. To this end, we first use recent algorithmic advances [29] to quantify the broadband focusing efficiency of macroscopic nanocomposite-enabled DLs and investigate within what range of NAs they can maintain a high performance. Subsequently, we derive analytic relationships for hybrid systems that connect the DL's numerical aperture ( $\text{NA}^{\text{dif}}$ ) and spatial structure to the overall system's NA. Furthermore, we present prototypical optical designs and perform wave optical simulations of diffractive and hybrid systems to confirm our results. Our analysis is valid for all technologies for DLs (e.g. échelette-type DLs, multi-level DLs, and metalenses) and shows that high-NA DLs are not required for broadband optical systems. In fact, high-NA DLs are even detrimental to the performance of such systems.

## 2. The potential and challenges of diffractive lenses

High-end imaging systems generally have contrast requirements of around 1/100 regarding stray light. This implies that only 1% of all light is allowed to reach the sensor as stray light. However, in optical design (e.g. in [2]), a DL is commonly treated as a perfect phase plate with an efficiency of 100% and no attention is paid as to how such a DL can be realized physically. On the other hand, studies into DLs often neglect the fact that complicated systems composed of several optical elements are required to achieve high quality imaging at higher NAs and larger apertures [35, 36]. To be able to reconcile these different points of view and analyze the requirements on DLs in optical systems, we here first recap the most important properties of DLs from both perspectives. Throughout this paper we use the terms DOE and DL as umbrella terms for all diffractive technologies (including metagratings and metalenses), since these different devices are different structural implementations for the same functionality.

### 2.1. Optical design perspective

In optical design, a DL is commonly described by its spatially dependent phase profile, which exerts its effect in an infinitely thin layer. For a spherical lens with a focal length of  $f(\lambda)$  the phase profile can be written as [2]:

$$\phi(r) = -\frac{\pi}{\lambda f(\lambda)} r^2, \quad (1)$$

where  $r$  is the radial distance from the center and we chose  $\phi(0) = 0$ . The wavelength dependence of a DL's focal length consequently reads  $f(\lambda) = \frac{1}{P(\lambda)} = \frac{\lambda_0}{\lambda} f(\lambda_0)$ , where  $P(\lambda)$  is the DL's refractive power. In refractive optics, the dispersion of an optical material is commonly quantified using its Abbe number ( $\nu_d = (n_d - 1)/(n_F - n_C)$ ) and partial dispersion ( $P_{g,F} = (n_g - n_F)/(n_F - n_C)$ ) [35], where the subscripts g, F, D, and C refer to the corresponding Fraunhofer spectral lines ( $\lambda_g = 435.83 \text{ nm}$ ,  $\lambda_F = 486.13 \text{ nm}$ ,  $\lambda_d = 587.56 \text{ nm}$  and  $\lambda_C = 656.28 \text{ nm}$ ). In fact, the focal shift between  $\lambda_F$  and  $\lambda_C$  of a single lens is determined by its material's Abbe number according to  $\Delta f_{F,C} = f_d/\nu_d$ . In turn,  $P_{g,F}$  additionally quantifies the focal shift at  $\lambda_g$  [35]. Using the  $\lambda^{-1}$  dependence of a DL's focal length, effective values of  $\nu_d$  and  $P_{g,F}$  can be assigned to a DL [2]:

$$\nu_d^{\text{dif}} = -3.452 \text{ and } P_{g,F}^{\text{dif}} = 0.2956. \quad (2)$$

We use the superscript 'dif' throughout this paper to indicate the properties of DLs. Note that the values of  $\nu_d^{\text{dif}}$  and  $P_{g,F}^{\text{dif}}$  follow directly from the phase profile that is given in equation (1) [2]. In good approximation, they are independent of how the DL is realized, that is, of what materials the DL is composed. The comparison of a DL's effective Abbe number ( $\nu_d^{\text{dif}}$ ) to those of conventional optical materials (figure 1(b)) shows that the chromatic aberrations induced by DLs are opposite in sign

and much larger compared to refractive lenses. Furthermore, it is evident from figure 1(b) that a DL has a highly anomalous effective partial dispersion ( $P_{g,F}^{\text{dif}}$ ), in that, its partial dispersion differs strongly from that of conventional optical materials. Since high-quality broadband imaging systems must be corrected for chromatic aberrations, it is critical to account for these properties in the design process. Below we show that this has profound implications for the integration of DLs into broadband optical systems.

In this context, we note that recently achromatic metalens singlets that are characterized by other values of  $\nu_d^{\text{dif}}$  and  $P_{g,F}^{\text{dif}}$  have been demonstrated [39–41]. Achromatic focusing performance has also been reported for multilevel DLs [42]. However, while achromatic singlets could be useful for certain applications, the efficiencies of such devices are far below those required to fulfill the contrast requirements of high-end imaging systems. This is because the efficiencies of achromatic metalenses and multilevel DLs have generally remained below 50% until now [39–42]. In fact, since these approaches rely on spatially discretizing the phase profiles, which need to be tailored for each wavelength individually, it appears likely that achieving efficiencies of close to 100% over a broad wavelength range will turn out to be an insurmountable challenge for such devices. Furthermore, we emphasize that a single flat lens that provides aberration-free imaging across a finite field of view (FOV) cannot exist since a flat lens cannot fulfill the Abbe sine condition [16, 25, 36]. Therefore, the currently most promising approach is to exploit the unique dispersion properties of DLs by integrating them into hybrid systems, that is, systems that include both refractive and diffractive elements.

## 2.2. DOE design perspective

After the phase profiles are determined in the optical design process, the key task for the ‘DOE-design’ is to find real devices that implement the required phase profiles. In fact, the phase delays that can be achieved in thin structures are fundamentally limited. Therefore, DOEs are generally designed by removing unnecessary multiples of  $2\pi$  from the continuous phase profile and instead varying the phase only between 0 and  $2\pi$  (figure 1(a)). However, this introduces recurring steps in the phase profile, which lead to the appearance of different diffraction orders. Spurious diffraction orders are suppressed if the phase delay across each segment changes linearly between 0 and a multiple of  $2\pi$  [43]. While this condition can be readily fulfilled for a single wavelength using so-called blazed gratings [10], the fact that dispersion causes the DOE’s phase profiles to be a function of the wavelength leads to phase differences that differ from  $2\pi$  for other wavelengths [43]. This generally leads to a strong wavelength dependence of the diffraction efficiency ( $\eta$ ) [26]. In addition, the efficiencies of real devices also depend on the grating period and the AOI, since their finite heights cause the phase delays to depend on the AOI and lead to shadowing at the boundaries between the segments [20, 26, 44]. To quantify the overall performance of a DOE within the visible spectral range ( $400 \text{ nm} \leq \Lambda \leq 800 \text{ nm}$ ), we define the

average efficiency within this wavelength range as  $\eta_{\text{PIDE}} = \frac{1}{\lambda_2 - \lambda_1} \int_{\lambda_1}^{\lambda_2} \eta(\lambda) d\lambda$  with  $\lambda_1 = 400 \text{ nm}$  and  $\lambda_2 = 800 \text{ nm}$  (polychromatic integral diffraction efficiency (PIDE)). However, our analysis can be readily generalized to other wavelengths by redefining  $\lambda_1$  and  $\lambda_2$ . Furthermore, for non-uniformly distributed light sources, the wavelength-dependent efficiencies ( $\eta(\lambda)$ ) in our definition of  $\eta_{\text{PIDE}}$  can be weighted by an additional wavelength-dependent factor. This can lead to relaxed requirements on DOEs in applications that operate within a narrower spectral range. In conclusion, the fact that the efficiency highly depends on the wavelength, AOI, and grating period illustrates that the widespread integration of DLs into real-world optical system will only become possible, if technologies for diffractive elements are developed that provide sufficiently high efficiencies across the parameter range that is required for a wide range of systems.

## 3. Nanocomposite-enabled diffractive lenses

As aforementioned, the first requirement for the integration of DOEs into broadband optical systems is overcoming the wavelength dependence of the efficiency. This is commonly referred to as ‘efficiency achromatization’ and several approaches have been developed for this purpose [9]. Our concept of nanocomposite-enabled EGs [26] builds on the ‘common depth’ approach [9, 45, 46] visualized in figure 1(d), and uses the dispersion-engineering capabilities of nanocomposites to tailor the magnitude and wavelength dependence of the refractive indices of the two layers ( $n_1(\lambda)$  and  $n_2(\lambda)$ ) such that the phase profile’s dispersion is almost perfectly cancelled out. In [26], we showed using numerical simulations of Maxwell’s equations that nanocomposite-enabled EGs can maintain unprecedented high average efficiencies of close to 100% across the entire visible range as well as a wide range of grating periods and AOIs. However, because of the high demands of full wave optical simulations on computational power and memory, we have so far only evaluated the performance of nanocomposite-enabled EGs for infinitely periodic structures. A systematic evaluation of the performance of nanocomposite-enabled DLs for full macroscopic lenses is still missing. In fact, the simulations for infinitely periodic structures in [26] showed that even the ideal design can only maintain high efficiencies for grating periods above  $20 \mu\text{m}$ . Since this threshold corresponds to a deflection angle of merely  $1.69^\circ$  at perpendicular incidence and a wavelength of  $0.588 \mu\text{m}$ , this limit imposes severe constraints on the refractive power a nanocomposite-enabled DL can provide. In fact, it has been shown that metagratings and metalenses can outperform conventional EGs for short grating periods and high NAs, respectively [16, 20, 22]. Furthermore, more recently, high-NA multilevel DLs with even higher efficiencies than metalenses have been demonstrated [13]. To answer the question of which of these technologies is best suited for such systems, we therefore investigate what parameter range is required to address the needs of broadband imaging systems in section 4.

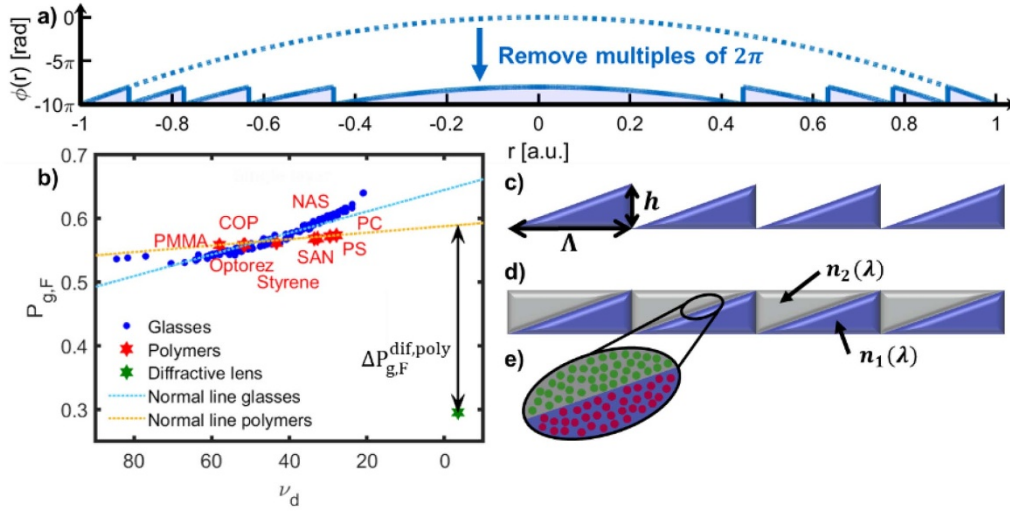


**Figure 1.** (a) Scheme of a diffractive lens (DL). (b) Partial dispersion ( $P_{g,F}$ ) as a function of the Abbe number ( $\nu_d$ ) for different materials and a DL. The diagram includes the Schott glasses (blue dots) [37], common optical polymers (red stars) [38], and the effective properties of a DL (green star). The lines represent the normal lines for the two material classes (poly(methyl methacrylate) (PMMA), cyclic olefin copolymer (COP), polystyrene (PS), polycarbonate (PC)). (c) Schemes of a single layer (SL) and (d) a common depth (CD) échelette-type grating (EGs). (e) The concept of nanocomposite-enabled EGs builds on the common depth approach depicted in (d) and uses the dispersion-engineering capabilities of nanocomposites to tailor  $n_1(\lambda)$  and  $n_2(\lambda)$  such that almost perfectly achromatic phase and hence efficiency profiles are achieved.

**Table 1.** Specifications of the EG designs (taken from [26]).

Type	Mat. 1	Mat. 2	Height ( $h$ )	$\eta_{PIDE,TEA}$
Single-layer (SL)	PMMA	Air	1.1 $\mu\text{m}$	86.93%
Nanocomposite-enabled (NE)	$f = 34.3\%$ diamond in PMMA	$f = 35\%$ ITO in PMMA	3.5 $\mu\text{m}$	99.96%
Common depth (CD)	N-BaF52	PC	26.3 $\mu\text{m}$	96.91 %

### 3.1. Macroscopic diffractive lenses (DLs)

To quantify the performance of macroscopic DLs, we here use a Matlab implementation of the recently introduced rotationally symmetric formulation of the wave propagation method (WPM) [29]. This method has been shown to be an efficient and accurate approach for evaluating the performance of DLs based on EGs [29]. As a prototype system for nanocomposite-enabled DLs, we here use the optimal material combination from [26]. In addition, we use a single-layer DL (figure 1(c)) for comparison. Finally, to show that novel dispersion engineered materials are essential for achieving a high performance, we later additionally investigate a state-of-the-art common depth DL (figure 1(d)). This DL is composed only of conventional optical materials [9, 45, 46]. The compositions of all three DLs are summarized in table 1. Note that the values of  $\eta_{PIDE}$  listed in table 1 correspond to the theoretical limits, which are achieved within the thin element approximation (TEA) [26].

To first visualize the general properties of DLs and highlight the difference between a single-layer and a

nanocomposite-enabled device, figure 2 depicts the propagation of light behind DLs based on the single-layer EG (figure 2(a)) and the nanocomposite-enabled EG (figure 2(b)). The different colors in the RGB images correspond to different wavelengths in the respective spectral ranges (red ( $\lambda_C$ ), green ( $\lambda_d$ ), and blue ( $\lambda_F$ )). We designed the lenses for a focal length of  $f(\lambda_d) = 30\text{mm}$  using equation (1) and fixed the aperture at  $D = 2\text{mm}$ . For each wavelength, we then performed a coherent simulation using the WPM and applied the logarithm of the resulting intensity distribution directly to the respective color channel. As the initial field we used  $E(r, z = 0) = E_0 \exp\left(-\left(\frac{2r}{\sigma_{\text{source}}}\right)^{20}\right)$ , where  $\sigma_{\text{source}}$  denotes the width of the beam. We used this super-Gaussian function with an exponent of 20, because it is flat in the center, but decays rapidly from its maximum to zero around  $r = \sigma_{\text{source}}/2$ . Therefore, it is a good approximation for a flat-top intensity profile. Furthermore, we used  $\sigma_{\text{source}} = 0.9 \times D$  to ensure that the field vanishes at the edge of the lens. This approach allows us to model a collimated beam of light and decreases the effective (i.e. illuminated) aperture of the system by 10%. The results of these simulations in figure 2 show that the different wavelengths have different focal lengths because of the previously discussed wavelength dependence of a DL's focal length (longitudinal chromatic aberration). More importantly, however, the single-layer structure (figure 2(a)) exhibits distinct higher order foci (white arrows), which are not visible for the nanocomposite-enabled device.

### 3.2. Focusing efficiency

Figure 2(a) visualizes that the appearance of spurious foci leads to stray light and consequently a loss of contrast in

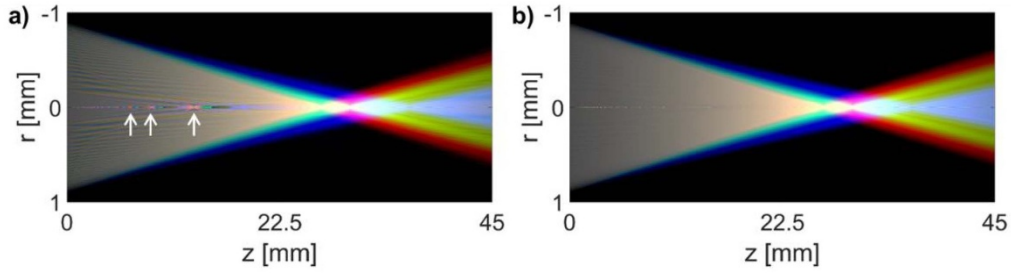


**Figure 2.** RGB images visualizing the propagation of light behind DLs with  $f = 30$  mm and  $D = 2$  mm for (a) the single-layer structure and (b) the nanocomposite-enabled device from table 1. The different color channels correspond to the logarithm of the spatial intensity distribution at the respective wavelength (red ( $\lambda_C$ ), green ( $\lambda_d$ ), and blue ( $\lambda_F$ )). The white arrows in (a) highlight the positions of the 2nd, 3rd, and 4th order foci for  $\lambda_C$ .

imaging systems. Therefore, as a measure of a DL’s performance, we define the focusing efficiency ( $\eta^{\text{foc}}$ ) as the fraction of the incident power that is focused into the desired focal spot. In practice, this quantity is difficult to evaluate precisely, because, even in the diffraction limit, the intensity pattern is infinitely extended. Moreover, the size of the focal spot generally depends on the wavelength and the specifications of the lens ( $f$  and  $D$ ) because of aberrations. Furthermore, the diffraction limit also increases with the wavelength. To account for these effects, we numerically approximate  $\eta^{\text{foc}}$  using the procedure visualized in figure 3(a): we first fit a Gaussian function to the central peak of the diffraction pattern in the focus plane and then determine the integrated intensity within a disk with a radius of  $r^{\text{foc}} = c_{\text{foc}} \times \sigma_{\text{Gauss}}$ , where  $\sigma_{\text{Gauss}}$  corresponds to the full  $e^{-2}$ -width of the Gaussian function and  $c_{\text{foc}}$  is a factor that we determine later. Finally, we divide this result by the integrated intensity directly behind the lens. Since the diffraction pattern in the focus is infinitely extended, the theoretical maximum for the focusing efficiencies that we obtain from this procedure is below 100% in any case. As a benchmark, we therefore use a refractive lens with a focal length of  $f = 30$  mm. This allows us to quantify the theoretical limit for the focusing efficiency in the absence of spurious diffraction orders. We then determined the factor  $c_{\text{foc}}$  in our definition of  $r^{\text{foc}}$  such that a focusing efficiency of  $\eta^{\text{foc}} \approx 0.99$  is achieved for the refractive lens. Doing so led us to a value of  $c_{\text{foc}} = 8$ . Note that we use the fitting procedure and not a fixed value for  $r^{\text{foc}}$ , which was the definition used in [29], to account for the broadening of focal spot due to aberrations. This allows us to separate changes in the focusing efficiencies from the broadening of the focal spot caused by other influences. Accordingly, figure 3(b) depicts  $\eta^{\text{foc}}$  as a function of the wavelength ( $\lambda$ ) for both the single layer and the nanocomposite-enabled DLs. For both DLs, this figure includes the data for two focal lengths of  $f = 30$  mm and  $f = 4$  mm. It is evident that, at  $f = 30$  mm, the nanocomposite-enabled DL can provide almost perfect broadband focusing and is distinguished by an essentially flat efficiency profile throughout the entire visible spectral range. In contrast, the single layer device’s efficiency drops rapidly towards the edges of the spectrum. In fact, these efficiency profiles closely resemble those obtained for the corresponding infinitely periodic structures [26]. As demonstrated by the dotted lines in figure 3(b), this is no longer the case at a

focal length of  $f = 4$  mm. However, the comparison of the two efficiency curves shows that the nanocomposite-enabled DL is still distinguished by a much flatter efficiency profile and hence still outperforms the single-layer device even at shorter focal lengths. To investigate these effects systematically, we define the polychromatic integral focusing efficiency ( $\eta_{\text{PIDE}}^{\text{foc}}$ ) as the average focusing efficiency between  $\lambda = 0.4 \mu\text{m}$  and  $\lambda = 0.8 \mu\text{m}$ . Throughout this paper, we numerically determine this quantity by sampling the wavelength in 50 nm intervals. Accordingly, figure 3(c) depicts  $\eta_{\text{PIDE}}^{\text{foc}}$  as a function of the focal length for the different DLs. It is evident that the  $\eta_{\text{PIDE}}^{\text{foc}}$  of the nanocomposite-enabled DL converges to the theoretical limit (dotted black line) for long focal lengths but decreases rapidly for focal lengths below 15 mm. In contrast, the  $\eta_{\text{PIDE}}^{\text{foc}}$  of the single layer structure converges to a much lower maximum, yet remains close to this limit across a wider range of focal lengths. Finally, the results for the common depth DL with conventional optical materials (yellow line in figure 3(c)) show that this structure’s  $\eta_{\text{PIDE}}^{\text{foc}}$  remains below 90% throughout the entire range of focal lengths. This highlights that novel dispersion-engineered materials are essential for achieving high focusing efficiencies. In fact, for infinitely periodic structures, we have recently investigated this relationship in detail and developed a general formalism for how the dispersion must be tailored for the design of highly efficient DOEs [33].

### 3.3. Role of the numerical aperture (NA)

The drop of the efficiency with decreasing focal lengths can be intuitively understood from the fact that shorter focal lengths require larger diffraction angles and hence shorter segment widths. This leads to a higher amount of shadowing. In fact, a DL’s minimum segment width consequently affects its focusing efficiency the most and should therefore be a good measure for a DL’s overall performance. To determine a DL’s minimum segment width, we start from equation (1) and calculate the number of segments within a radius of  $r$ :

$$N_{\text{seg}}(r) = \frac{|\phi(r)|}{2\pi} = \frac{r^2}{2\lambda_0 |f(\lambda_0)|}. \quad (4)$$

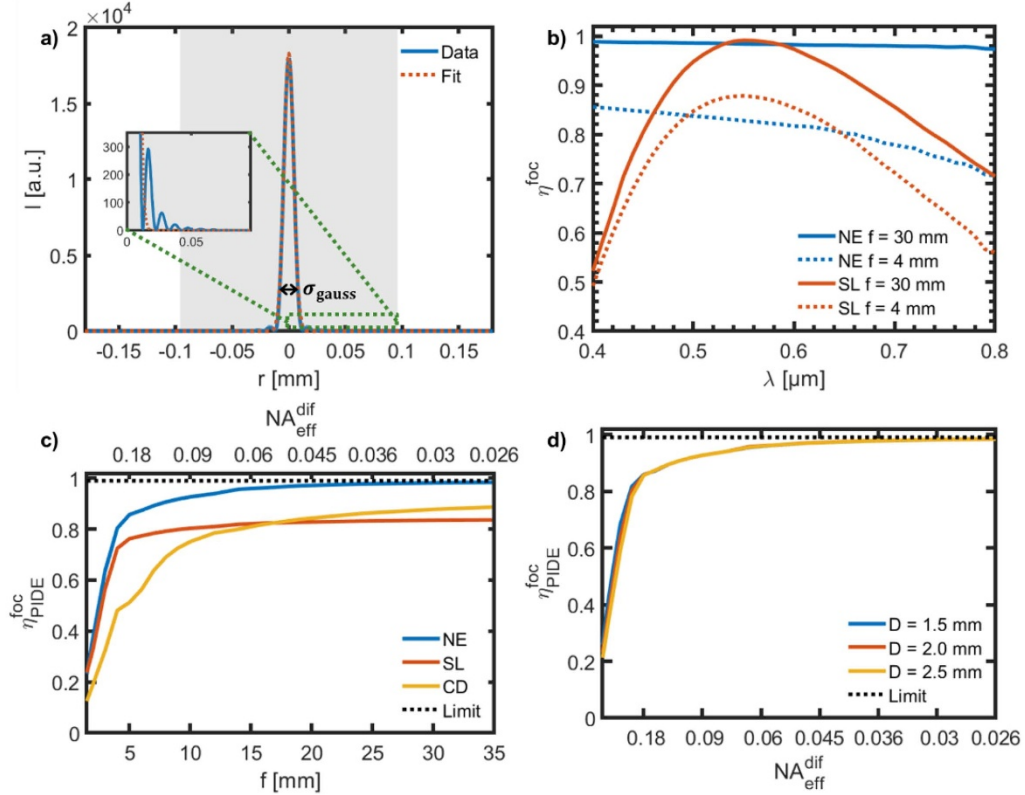


**Figure 3.** (a) Procedure for determining the focusing efficiency ( $\eta^{\text{foc}}$ ): the dashed red line depicts the Gaussian function ( $e^{-2}$ -width:  $\sigma_{\text{Gauss}}$ ) that was fitted to the central peak to determine the radius of the focus ( $r^{\text{foc}} = 8 \times \sigma_{\text{Gauss}}$ ). The grey area visualizes the range  $r \leq r^{\text{foc}}$  that was used to determine the integrated intensity within the focus. (b)  $\eta^{\text{foc}}$  as a function of the wavelength for the nanocomposite-enabled (NE) and the single layer (SL) DL at different focal lengths ( $f$ ). (c) Average focusing efficiency within the visible spectral range ( $\eta_{\text{PIDE}}^{\text{foc}}$ ) as a function of  $f$  at an aperture of  $D = 2$  mm for both devices and a state-of-the-art common depth (CD) DL without dispersion-engineered materials. (d)  $\eta_{\text{PIDE}}^{\text{foc}}$  of the nanocomposite-enabled DL over  $\text{NA}_{\text{eff}}^{\text{dif}} = 2f/D$  for different apertures.

The spatial frequencies of the segments ( $k_{\text{seg}}$ ), and their widths ( $\Lambda(r)$ ) now follow directly from the derivative of  $N_{\text{seg}}(r)$ :

$$k_{\text{seg}}(r) = \frac{d}{dr} N_{\text{seg}}(r) = \frac{r}{\lambda_0 |f(\lambda_0)|}, \text{ and } \Lambda(r) = \frac{1}{k_{\text{seg}}(r)} = \frac{\lambda_0 |f(\lambda_0)|}{r} \quad (5)$$

Equation (5) shows that the shortest segment ( $\Lambda_{\text{min}}^{\text{dif}}$ ) appears at the edge of DLs ( $r = R$ ):

$$\Lambda_{\text{min}}^{\text{dif}} = \Lambda(R) = \frac{\lambda_0 |f(\lambda_0)|}{R} \approx \frac{\lambda_0}{\text{NA}_{\text{eff}}^{\text{dif}}}, \quad (6)$$

which proves that, for a given design wavelength ( $\lambda_0$ ),  $\Lambda_{\text{min}}^{\text{dif}}$  is solely determined by the ratio  $\frac{f}{R} = \frac{2f}{D} = 2N_f^{\text{dif}} \approx \frac{1}{\text{NA}_{\text{eff}}^{\text{dif}}}$ , where  $N_f^{\text{dif}}$  is the lens' f-number. In addition, we used the approximate relationship  $\text{NA} \approx \frac{1}{2N_f}$  for the numerical aperture [47]. Since the numerical aperture and the f-number are quantities that are commonly only assigned to more complicated optical systems, we here use the superscript 'dif' to indicate if they refer to a single DL. In figure 3(c), the upper x-axis directly denotes the  $\text{NA}_{\text{eff}}^{\text{dif}}$  for each focal length. Here and in the following we use the subscript 'eff' to indicate that we accounted for the fact that only 90% of the physical aperture is illuminated.

The upper x-axis in figure 3(c) demonstrates that the  $\eta_{\text{PIDE}}^{\text{foc}}$  of the nanocomposite-enabled DL starts to deviate noticeably from the theoretical limit around  $\text{NA}_{\text{eff}}^{\text{dif}} \approx 0.03$ . Equation (6) yields that this corresponds to a minimum segment width of  $\Lambda_{\text{min}}^{\text{dif}} \approx 20 \mu\text{m}$ , which is also where the simulations with periodic boundary conditions predict a significant drop of the performance [26].

To confirm that the focusing efficiency of a DL is determined only by its NA ( $\text{NA}^{\text{dif}}$ ) and not the size of the lens independently, figure 3(d) presents the  $\eta_{\text{PIDE}}^{\text{foc}}$  of the nanocomposite-enabled DL as a function of its NA for different diameters of the aperture ( $D$ ). It is evident that there are only minimal differences between the efficiencies obtained for the different apertures at larger values of  $\text{NA}^{\text{dif}}$ . These minor differences can be attributed to the fact that our procedure for determining the focusing efficiency exhibits a weak residual dependence on the increase of spherical aberration with increasing aperture. This analysis hence shows the nanocomposite-enabled device can provide essentially perfect broadband focusing up to  $\text{NA}_{\text{eff}}^{\text{dif}} \approx 0.03$ . For higher values of  $\text{NA}_{\text{eff}}^{\text{dif}}$ , spurious foci start to appear that lead to stray light. In fact, this restriction to small values of  $\text{NA}^{\text{dif}}$  can be regarded as a fundamental limit for DLs based on EGs. This is because the heights of EGs are determined by the refractive index differences between the layers,

which, in turn, underly fundamental limits [33, 48]. Therefore, the crucial question is whether the upper limit of  $NA^{dif} = 0.03$  is sufficient for the integration of nanocomposite-enabled DLs into high-quality broadband optical systems.

#### 4. DOEs in broadband optical systems

High-quality broadband imaging systems must be corrected for chromatic aberrations. This makes it essential to account for the strong and anomalous chromatic properties ( $\nu_d^{dif}$  and  $P_{g,F}^{dif}$ ) of DLs in the design process [2]. In fact, since a (highly efficient) DL is characterized by fixed values of  $\nu_d^{dif}$  and  $P_{g,F}^{dif}$ , the correction of chromatic aberrations requires both refractive and diffractive elements. Furthermore, we emphasize again that a single flat lens that provides aberration-corrected monochromatic imaging of finite sized objects cannot exist [36]. Therefore, the key task for the integration of DLs into optical systems is not to realize DLs with high values of  $NA^{dif}$ , but rather to design DLs that have precisely the amount of refractive power required to minimize the chromatic aberrations in the systems. In addition, it is critical to keep the amount of stray light that reaches the sensor at level at which the contrast requirement of the overall system can be fulfilled. It is consequently indispensable to quantitatively investigate what values of  $NA^{dif}$  and  $\Lambda_{min}$  are required for broadband systems. To do so, we here first analytically investigate the requirements on DLs in hybrid achromats and apochromats. For these systems, we can build on the analytical relationships derived in [2], where hybrid achromats and apochromats have been investigated from the ‘optical design perspective’, that is, without taking the microscopic structure and the efficiencies of the DLs into account.

##### 4.1. Hybrid achromats

The simplest system that is corrected for chromatic aberrations is an achromat. An achromat is a two-element system that has the same focal length at two wavelengths ( $f(\lambda_0) = f(\lambda_1)$ ). The total refractive power of an achromat consisting of one refractive and one diffractive element reads  $P^{acr}(\lambda) = \frac{1}{f^{acr}(\lambda)} = P^{dif}(\lambda) + P^{ref}(\lambda)$ . Here, we use the superscripts ‘acr’ and ‘ref’ to denote the properties of achromats and refractive lenses, respectively. In the visible spectral range, a suitable choice for the two wavelengths is  $\lambda_0 = \lambda_F$  and  $\lambda_1 = \lambda_C$ . To investigate the properties of a DL in an achromat we start from the equations derived in [2]:

$$f^{dif} = f^{acr} \left( \frac{\nu_d^{dif} - \nu_d^{ref}}{\nu_d^{dif}} \right) \text{ and } f^{ref} = f^{acr} \left( \frac{\nu_d^{ref} - \nu_d^{dif}}{\nu_d^{ref}} \right), \quad (7)$$

where we omitted the argument  $\lambda_d$  for all focal lengths. If we now introduce ratio between  $\nu_d^{dif}$  and  $\nu_d^{ref}$  according to  $\nu_d^{ref} = -q^{acr} \nu_d^{dif}$  with  $q > 0$  these relationships simplify to:

$$f^{dif} = f^{acr} (1 + q^{acr}) \text{ and } f^{ref} = f^{acr} \left( \frac{1 + q^{acr}}{q^{acr}} \right). \quad (8)$$

If we then replace the focal lengths by the respective NAs we arrive at:

$$NA^{dif} = \frac{NA^{acr}}{(1 + q^{acr})} \text{ and } NA^{ref} = NA^{acr} \left( \frac{q^{acr}}{1 + q^{acr}} \right), \quad (9)$$

which proves that  $NA^{dif}$  is a factor of  $(1 + q^{acr})^{-1}$  smaller than  $NA^{acr}$ . Finally, substituting this result for  $NA^{dif}$  into equation (6) leads us to an expression for the minimum segment width of a DL in a hybrid achromat ( $\Lambda_{min}^{acr}$ ):

$$\Lambda_{min}^{acr} = \frac{\lambda}{NA^{acr}} (1 + q^{acr}). \quad (10)$$

The minimum segment width required from the DL consequently increases by a factor of  $(1 + q^{acr})$  compared to a diffractive singlet with the same NA. To quantitatively estimate  $q^{acr}$ , we can use common material choices for positive lenses, which, for example, are N-BK7 for systems comprised of glasses or PMMA for systems made of polymers. The Abbe numbers of these materials are  $\nu_d^{BK7} = 64.17$  [37] and  $\nu_d^{PMMA} = 58.00$  [38], which yields  $q_{PMMA}^{acr} = 16.80$  and  $q_{BK7}^{acr} = 18.59$ , respectively. This shows that, for common material choices,  $NA^{dif}$  is more than an order of magnitude smaller than the numerical aperture of the overall hybrid system ( $NA^{acr}$ ) and hence proves that DLs with high values of  $NA^{dif}$  are not required for hybrid achromats. In fact, it follows from equation (9) that the limit of  $NA^{dif} = 0.03$  up to which nanocomposite-enabled DLs can provide perfect broadband focusing allows for the design of hybrid achromats with  $NA^{acr} \leq 0.53$  for PMMA or even  $NA^{acr} \leq 0.59$  for N-BK7. These values correspond to f-numbers of  $N_f \geq 0.94$  and  $N_f \geq 0.85$ , respectively. This range hence already covers the range of high-end camera lenses [35], and we show below that this situation improves even further for more complicated systems whose chromatic aberrations are corrected to a higher degree.

To investigate the performance of a prototype hybrid achromat with a nanocomposite-enabled DL and confirm the validity of the equations derived above, we used the optical design software ‘OpticStudio’ to design a hybrid achromat with  $f^{acr}(\lambda_d) = 4\text{mm}$ , and  $D = 2\text{mm}$  ( $NA^{acr} = 0.25$ ). This value of  $NA^{acr}$  corresponds to the upper limit for which the system can still maintain diffraction-limited performance. For higher values of  $NA^{acr}$ , spherical aberration affects the achromat’s performance. After we optimized the system in ‘OpticStudio’ using ray tracing, we implemented the optimized structure into Matlab and again performed a wave-optical simulation using the WPM. Figure 4(a) presents an RGB image visualizing the propagation of polychromatic light through the optimized achromat. We again used the procedure described in section 3 to obtain this image and used the nanocomposite-enabled structure (table 1) for the DL. The DL’s structure in figure 4(b) illustrates that it has a minimum segment width of  $\Lambda_{min}^{acr} = 39\mu\text{m}$ , which agrees well with the value of  $\Lambda_{min}^{acr} = 42\mu\text{m}$  predicted by equation (10). The small difference can mostly be attributed to the achromat’s finite thickness. Since this minimum segment width corresponds to a value of  $NA^{dif} = 0.015$  (equation (7)), this confirms that the

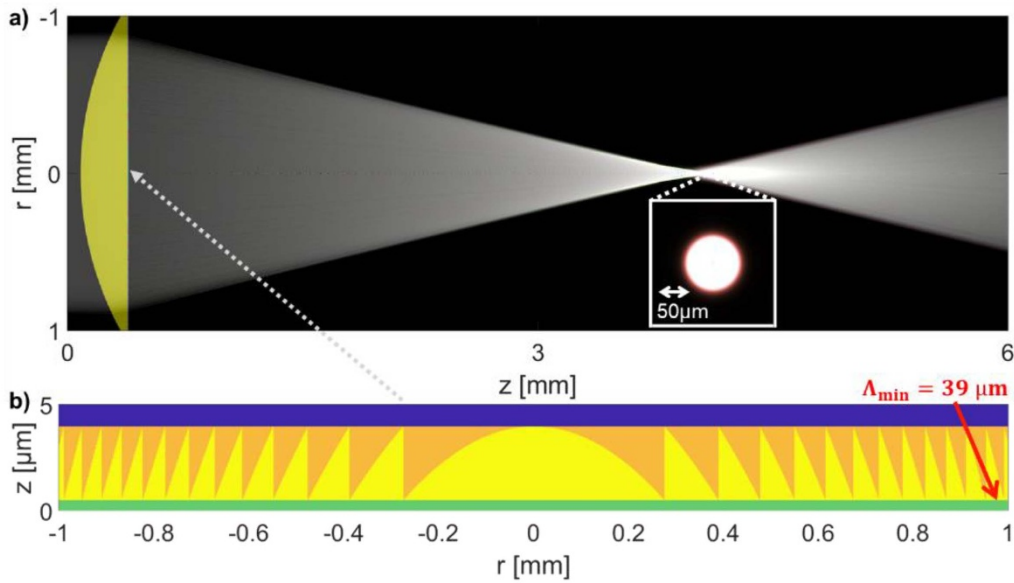


**Figure 4.** (a) Light propagation through a hybrid achromat comprised of PMMA with a focal length of  $f^{\text{acr}}(\lambda_d) = 4 \text{ mm}$  and  $\text{NA}^{\text{acr}} = 0.25$  (details on how this image was obtained in description of figure 3). The inset visualizes the intensity distribution in the focus plane for backlighting (a heavily saturated sensor). (b) Structure of the nanocomposite-enabled DL (see table 1), which is placed on the refractive lens' flat second surface. The different colors denote the four materials (green: PMMA; yellow: diamond in PMMA nanocomposite; orange: ITO in PMMA nanocomposite; blue: air).

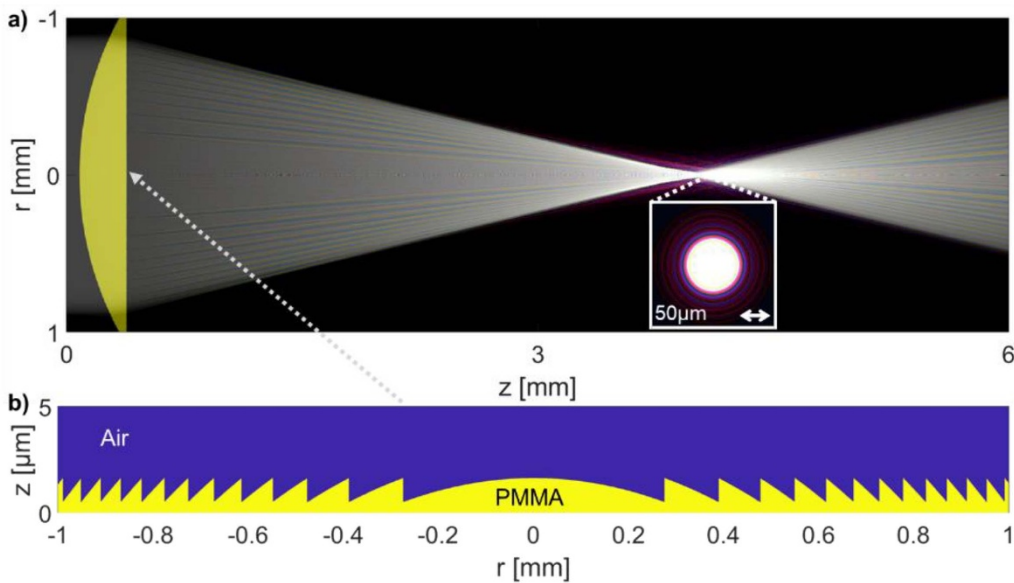


**Figure 5.** (a) Light propagation through the achromat from figure 4 with a single layer DL (structure in (b)) instead of the nanocomposite-enabled device (see table 1). The inset in (a) visualizes the intensity distribution in the focus plane for backlighting (a heavily saturated sensor) using the same scale as for figure 4. The different colors denote the two materials (yellow: PMMA; blue: air).

DL is operated in the regime in which the nanocomposite-enabled DL can provide perfect broadband focusing. This is confirmed by the lack of spurious foci in figure 4(a). To confirm that spurious diffraction orders remain suppressed even in the worst-case scenario of backlighting, that is, for a heavily saturated sensor, the inset in figure 4(a) visualizes the achromat's intensity profile in the focus plane under such conditions. It is evident that no spurious diffraction orders are observed in this image. There is only a weak red hue

around the spot, which can be attributed to the fact that the spot size in the diffraction limit increases with increasing wavelength.

#### 4.2. Efficiency requirements

The finding that a DL in a hybrid system must only provide little refractive power relaxes the requirements on the DL's NAs ( $\text{NA}^{\text{dif}}$ ). However, it also has a profound impact on

the efficiency requirements. This is because the less focusing power a DL in a hybrid system provides, the smaller the separation between the different orders becomes. This can be seen from figure 5(a), which again presents the propagation of light through the achromat from figure 4, but with the single-layer DL (figure 5(b)) instead of the nanocomposite-enabled DL (figure 4(b)). It is evident that, for this system, the influence of spurious diffraction orders is clearly visible as spurious colorful rays around the primary focus. The figure's inset additionally visualizes that this leads to colorful fringes in the focus plane under backlighting. This demonstrates that, if weakly focusing DLs are integrated into hybrid systems, the different orders will propagate so close to each other that most of the light in the spurious orders will reach the sensor. In fact, this can even lead to prominent ghost images. This visualizes that it can be assumed that almost all light in spurious diffraction orders in hybrid broadband systems reaches the sensor. Therefore, the contrast requirement of 1/100 of high-end optical systems can only be fulfilled if the focusing efficiency remains within around 1% of the theoretical limit. As shown previously, this condition can be fulfilled by the nanocomposite-enabled DL up to values of approximately  $NA^{dif} = 0.03$ , but not by the single-layer DL or common depth DL with conventional materials (figure 3).

#### 4.3. Hybrid apochromat

Achromats still exhibit a residual focal shift for wavelengths other than the two design wavelengths. This residual color error is usually referred to as the 'secondary spectrum' and its correction is essential for high-quality optical systems. In optical design, this is commonly called 'apochromatization'. An apochromat, in this sense, is a system that fulfills the condition  $f(\lambda_1) = f(\lambda_2) = f(\lambda_3)$  for three distinct wavelengths. In this paper, we choose  $\lambda_1 = \lambda_g$ ,  $\lambda_2 = \lambda_F$ , and  $\lambda_3 = \lambda_C$ . This choice ensures that we can use the Abbe number  $\nu_d$  and partial dispersion  $P_{g,F}$  in the following expressions. But our analysis can be straightforwardly generalized to other wavelengths. In general, hybrid apochromats consist of two refractive elements and one diffractive one. The individual focal lengths of the three elements can be calculated from [2]:

$$f^{ref,1} = f^{apo} \frac{E(\nu_d^{dif} - \nu_d^{ref,2})}{(P_{g,F}^{ref,2} - P_{g,F}^{dif})\nu_d^{ref,1}}, f^{ref,2} = f^{apo} \frac{E(\nu_d^{dif} - \nu_d^{ref,1})}{(P_{g,F}^{ref,1} - P_{g,F}^{dif})\nu_d^{ref,2}} \quad (11)$$

and

$$f^{dif} = f^{apo} \frac{E(\nu_d^{dif} - \nu_d^{ref,2})}{(P_{g,F}^{ref,1} - P_{g,F}^{ref,2})\nu_d^{dif}}, \quad (12)$$

where the factor  $E$  is defined as [2]:

$$E = \frac{\nu_d^{dif}(P_{g,F}^{ref,1} - P_{g,F}^{ref,2}) + \nu_d^{ref,1}(P_{g,F}^{ref,2} - P_{g,F}^{dif}) + \nu_d^{ref,2}(P_{g,F}^{dif} - P_{g,F}^{ref,1})}{\nu_d^{dif} - \nu_d^{ref,2}} \quad (13)$$

We use the superscript 'apo' to denote the properties of the overall apochromat. To investigate the properties of the DL in a hybrid

apochromat, we now first write the linear relationship that connects the locations of the two refractive elements' materials in the  $P_{g,F}$ -diagram as  $P_{g,F}^{ref}(\nu_d^{ref}) = \alpha + \beta\nu_d^{ref}$ . Furthermore, we introduce  $\Delta P_{g,F}^{dif}$  as the distance of  $P_{g,F}^{dif}$  from this line (figure 1(b)), and hence write  $P_{g,F}^{dif} = \alpha + \beta\nu_d^{dif} + \Delta P_{g,F}^{dif}$ . Substituting these relationships into equations (12) and (13) leads us to simple expressions for  $f^{dif}$  and  $NA^{dif}$ :

$$f^{dif} = -f^{apo} \frac{\Delta P_{g,F}^{dif}}{\beta\nu_d^{dif}} = f^{apo} q^{apo} \text{ and } NA^{dif} = \frac{NA^{apo}}{q^{apo}}, \quad (14)$$

where we introduced the factor  $q^{apo} = -\frac{\Delta P_{g,F}^{dif}}{\beta\nu_d^{dif}}$ , which is positive because  $\Delta P_{g,F}^{dif}$ ,  $\beta$ , and  $\nu_d^{dif}$  are all negative. In general, the slope  $\beta$  and the distance  $\Delta P_{g,F}^{dif}$  in equation (14) must be determined separately for each material combination according to:

$$\beta = \frac{P_{g,F}^{ref,2} - P_{g,F}^{ref,1}}{\nu_d^{ref,2} - \nu_d^{ref,1}} \text{ and } \Delta P_{g,F}^{dif} = P_{g,F}^{dif} - P_{g,F}^{ref,i} + \beta(\nu_d^{ref,i} - \nu_d^{dif}), \quad (15)$$

where  $i \in (1, 2)$ . However, for most optical glasses or polymers, the normal lines in figure 1(b) provide a good approximation. For glasses, this line is defined as the line that connects K7 and F2 [49]. By substituting equation (14) into equation (6), we finally find that the DL's minimum segment width also increases by  $q^{apo}$ :

$$\Lambda_{min}^{apo} = \frac{\lambda}{NA^{apo}} q^{apo}. \quad (16)$$

To estimate common values of  $q^{apo}$ , we first use the normal line for glasses and, second, we use the line that connects PMMA and PC for polymers (figure 1(b)). For the glasses K7 and F2, this leads to  $\beta^{glass} = -0.00168$  and  $\Delta P_{g,F}^{dif,glass} = -0.354$ , which results in a factor of  $q^{apo,glass} = 59.0$ . Furthermore, for the polymers PMMA and PC, we obtain  $\beta^{poly} = -0.000507$ ,  $\Delta P_{g,F}^{dif,poly} = -0.293$  and consequently even  $q^{apo,poly} = 164$ . These results prove that the values of  $NA^{dif}$  required for hybrid apochromats are around two orders of magnitude smaller than the NA of the overall system. Accordingly, the minimum segment width increases by the same factor compared to a diffractive singlet with the same NA. For the optical glasses, the limit of  $NA^{dif} = 0.03$ , up to which nanocomposite-enabled DLs maintain essentially perfect broadband focusing, hence covers the requirements of apochromats with NAs of up to  $NA^{apo} = 1.77$ . This range essentially encompasses all optical systems, even high-NA immersion systems. Conversely, to achieve  $NA^{apo} = 1$ , which is the theoretical maximum for the NA in air, a DL with a NA of merely  $NA^{dif} = 0.017$  ( $\Lambda_{min} = 34.7 \mu\text{m}$ ) or  $NA^{dif} = 0.0061$  ( $\Lambda_{min} = 96.4 \mu\text{m}$ ) is required for the optical glasses or polymers, respectively. In fact, below, we demonstrate that the relationships derived in this section also provide a good approximation for more complex apochromatic systems, which are composed of more than three optical elements. This shows that a nanocomposite-enabled DL in a high-end apochromatic system can be operated well below the limit

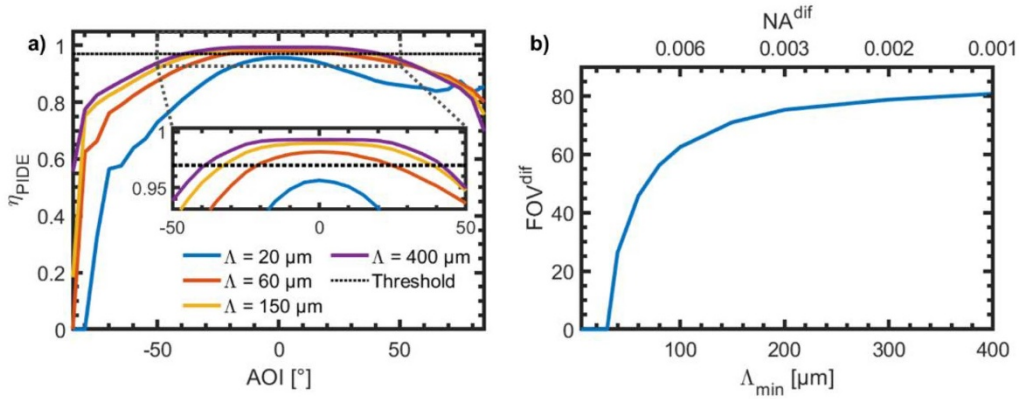


**Figure 6.** (a) Polychromatic integral diffraction efficiency ( $\eta_{\text{PIDE}}$ ) for the nanocomposite-enabled EG from table 1 assuming an infinitely periodic grating as a function of the AOI. As the surrounding medium air with  $n = 1$  was used. This data was obtained using the FEM software JCMsuite. The colors correspond to different grating periods and the dotted line visualizes the efficiency threshold of 97%. (b) Field of view of the EG ( $\text{FOV}^{\text{dif}}$ ) defined as the full range of AOIs across which  $\eta_{\text{PIDE}}$  remains above the efficiency threshold as a function of  $\Lambda = \Lambda_{\text{min}}$ . The upper x-axis denotes the corresponding value of  $\text{NA}^{\text{dif}}$  (equation (6)). Since for a DL most segments are much larger than  $\Lambda_{\text{min}}$  these values quantify the lower boundary for  $\text{FOV}^{\text{dif}}$ .

at which its efficiency is affected. High values of  $\text{NA}^{\text{dif}}$  are hence not required for broadband optical systems. In fact, high values of  $\text{NA}^{\text{dif}}$  would even be detrimental for the performance of such systems, since they would lead to drastically overcorrected chromatic aberrations. Note that this situation changes for monochromatic or very narrowband applications for which the color errors induced by a DL do not play a role.

#### 4.4. Field of view

So far, we have shown that nanocomposite-enabled DLs can achieve essentially perfect broadband focusing up to  $\text{NA}^{\text{dif}} = 0.03$  and that higher values of  $\text{NA}^{\text{dif}}$  are, in fact, not required for broadband optical systems. The final requirement for the integration of DLs into optical systems is that high efficiencies must also be maintained across the full range of AOIs that is incident on the DL within the system. This is because imaging of finite sized objects always requires a certain FOV, that is, a finite range of AOIs. In principle, it would be possible to introduce constraints on the AOIs at the DL's position in the optical system. However, such constraints would at least partly diminish the benefits of adding the DL. Therefore, accessing the full potential of DLs for optical systems requires devices that maintain high efficiencies across the system's full FOV or an even larger range of AOIs.

In sections 3.2 and 3.3, we have shown that a DL's minimum segment width ( $\Lambda_{\text{min}}$ ) is directly connected to its NA ( $\text{NA}^{\text{dif}}$ ) and hence directly determines the DL's performance. In fact, our analysis in section 3.2 (see figure 3) has demonstrated that the performance of a macroscopic DL begins to be affected if its minimum grating period ( $\Lambda_{\text{min}}$ ) reaches a value at which simulations of infinitely periodic structures predict a significant drop of the DL's performance. To quantify the range of AOIs across which DLs maintain a high performance, we can therefore use a periodic grating with a period of  $\Lambda = \Lambda_{\text{min}}$ . Since most of the DL consists of segments that

are much larger than  $\Lambda_{\text{min}}$ , this approach allows us to quantify a lower boundary for the DL. We here investigate infinitely periodic structures because the WPM becomes highly inefficient for oblique incidence because of the broken cylindrical symmetry. Furthermore, for oblique incidence, off-axis aberrations lead to highly distorted spots. This makes it difficult to accurately quantify the focusing efficiencies. Accordingly, figure 6(a) depicts the polychromatic integral diffraction efficiency ( $\eta_{\text{PIDE}}$ ) for the nanocomposite-enabled EG (table 1) as a function of the AOI for different grating periods. We obtained this data using the finite element method (FEM) software JCMsuite. Note that we used air with  $n = 1$  as the surrounding medium for these simulations, whereas we assumed the EG's materials to extend to infinity in [26, 33]. This leads to higher efficiencies for oblique incidence since the incident light is refracted at the additional interfaces according to Snell's law. Figure 6(a) shows that, for large grating periods the,  $\eta_{\text{PIDE}}$  remains almost flat across a broad range of AOIs. In contrast, for shorter grating periods, a more rapid decrease of the  $\eta_{\text{PIDE}}$  with increasing AOI is observed. To systematically quantify this relationship, we define the an EG's field of view ( $\text{FOV}^{\text{dif}}$ ) as the full range of AOIs across which the EG's  $\eta_{\text{PIDE}}$  remains above 97% (dotted black line in figure 6(a)). Figure 6(b) illustrates that the  $\text{FOV}^{\text{dif}}$  indeed drops rapidly with decreasing grating periods. However, values of  $\text{FOV}^{\text{dif}} \geq 75^\circ$  are achieved for  $\Lambda_{\text{min}} \geq 200 \mu\text{m}$  ( $\text{NA}^{\text{dif}} \leq 0.003$ ). Furthermore, at  $\Lambda_{\text{min}} = 100 \mu\text{m}$  ( $\text{NA}^{\text{dif}} = 0.006$ ), the EG still covers a FOV of  $\text{FOV}^{\text{dif}} = 62^\circ$ . These values exceed the FOVs that are required for a wide range of optical systems by far. For example, microscopes generally have FOVs below  $8^\circ$ , whereas photographic lenses span a much wider range from down to  $2^\circ - 4^\circ$  for extreme telephoto up to  $43 - 56^\circ$  for standard focal lengths [35]. Moreover, we emphasize again that our procedure of using a periodic grating with  $\Lambda = \Lambda_{\text{min}}$  to estimate the FOV of a DL with a minimum segment width of  $\Lambda_{\text{min}}$  can be expected to underestimate the DL's actual FOV. Therefore, our results demonstrate that

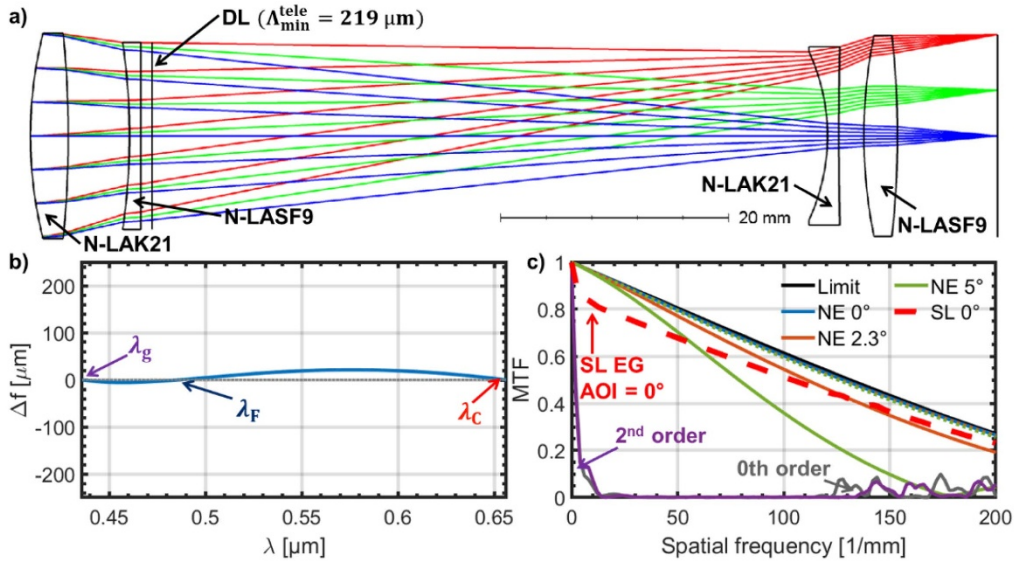


**Figure 7.** (a) Layout of a prototype telephoto lens with a focal length of  $f = 100$  mm, a f-number of  $N_f = 5.6$ , a field of view of  $FOV = 10^\circ$ , and a total length of  $TL = 85$  mm. The DL has a minimum segment width of  $\Lambda_{\min}^{\text{tele}} = 219 \mu\text{m}$  ( $NA^{\text{dif}} = 0.0027$ ). (b) Focal shift ( $\Delta f$ ) as a function of the wavelength to visualize that the system fulfills  $f(\lambda_g) = f(\lambda_F) = f(\lambda_C)$ . (c) Modulation transfer function (MTF) for three AOIs in both the tangential (solid lines) and sagittal planes (dashed lines) using the nanocomposite-enabled (NE) DL. The purple and grey lines additionally depict the MTF for the lowest order spurious foci. The dashed red line shows for  $AOI = 0^\circ$  that these spurious foci drastically affect the performance if the single layer (SL) DL is used.

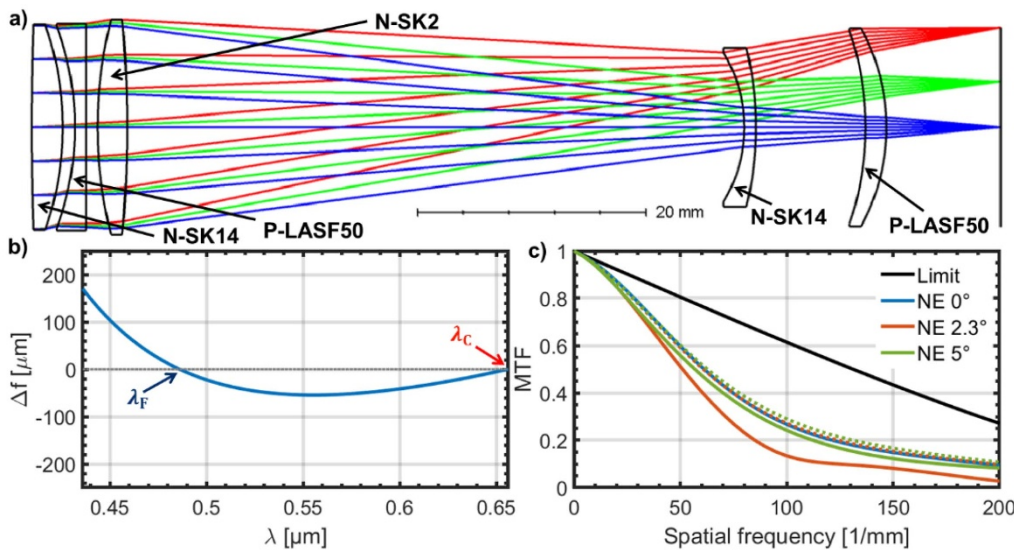


**Figure 8.** (a) Layout of a purely refractive telephoto lens with a focal length of  $f = 100$  mm, a f-number of  $N_f = 5.6$ , a field of view of  $FOV = 10^\circ$ , and a total length of  $TL = 85$  mm. This system serves as a benchmark system for the hybrid system presented in figure 7(b) Focal shift ( $\Delta f$ ) as a function of the wavelength to visualize that the system only fulfills  $f(\lambda_F) = f(\lambda_C)$ . (c) Modulation transfer function (MTF) for three AOIs in both the tangential (solid lines) and sagittal planes (dashed lines). The MTF is drastically decreased compared to the hybrid system.

nanocomposite-enabled DLs would indeed be suitable for most broadband imaging systems.

### 5. Prototype telephoto lens

Telephoto lenses suffer strongly from longitudinal chromatic aberrations because of their large focal lengths. As

already demonstrated in [4], integrating DLs into such systems therefore holds an immense potential. To show that nanocomposite-enabled DLs allow for unlocking the full potential of DLs for such systems, we designed an apochromatic telephoto system. This, at the same time, allows us to confirm our findings from section 3 for a more complex optical system. For this prototype system, we chose a focal length of  $f = 100$  mm, a f-number of  $N_f = 5.6$ , a field of view of  $FOV = 10^\circ$ , and a total length of  $TL = 85$  mm. We again chose these

parameters such that the system maintains close to diffraction-limited performance across the entire FOV. As evident from system's layout in figure 7(a), we designed the system with four refractive lenses. We chose four lenses because a telephoto lens, that is, a system with  $f > TL$  generally must be composed of at least a positive and a negative group [35]. To correct the system for chromatic aberration to the first degree both these groups must then be achromats themselves [35]. An achromatic telephoto system must hence be composed of at least four elements. Furthermore, we included the lens' materials in the optimization, but constrained the second group's materials to be the same as those of the first group. We chose this constraint because it represents the 'worst-case scenario' in which the DL must work against the dispersion from both groups to achieve apochromatization. Finally, we included no constraints on the DL and allowed it to freely move within the system.

To demonstrate that the optimized prototype system indeed fulfills the apochromatization condition ( $f(\lambda_g) = f(\lambda_F) = f(\lambda_C)$ ), figure 7(b) depicts its focal shift as a function of the wavelength. Because of the restriction to two materials, this would generally not be possible without the DL. Furthermore, the system's modulation transfer function (MTF) in figure 7(c) illustrates that the system provides close to diffraction limited performance at all spatial frequencies and across the entire FOV. Note that a system's MTF directly quantifies its contrast as a function of the spatial frequencies in the image. In fact, the prototype telephoto system's MTF remains completely unaffected by light in spurious diffraction orders if the nanocomposite-enabled DL is used in the system. This is because the unconstrained optimization of the DL lead to a minimum segment width of  $\Lambda_{\min}^{\text{tele}} = 219 \mu\text{m}$  (see figure 7(a)), which corresponds to a NA of  $\text{NA}^{\text{dif}} = 0.0027$ . Therefore, the DL is operated way below the limit of  $\text{NA}^{\text{dif}} = 0.03$  at which its performance is impaired. Furthermore, at these values of  $\Lambda_{\min}^{\text{tele}}$  and  $\text{NA}^{\text{dif}}$ , the DL has a  $\text{FOV}^{\text{dif}}$  that highly exceeds the system's FOV of  $10^\circ$  (figure 6). In fact, since the DL is operated an order of magnitude below the limit of  $\text{NA}^{\text{dif}} = 0.03$  at which its performance is affected, this prototype system demonstrates that nanocomposite-enabled DLs are indeed also suitable for much more complex systems with higher f-numbers and FOVs.

To illustrate that the performance of the prototype system is drastically affected if a significant amount of light reaches the DL's spurious foci, the grey and purple lines in figure 7(c) depict the MTF for the 0th and 2nd diffraction orders at an AOI of  $0^\circ$ . These data show that the MTF is almost zero for these spurious foci at essentially all spatial frequencies. If the focusing efficiencies are significantly below the theoretical limit, the influence of these spurious orders hence leads to a rapid drop of the system's performance. This is directly visualized by the dashed red line, which depicts the prototype telephoto system's MTF for an AOI of  $0^\circ$  if the single-layer DL is used instead of the nanocomposite-enabled DL. For this dashed red line, we used the result from figure 3(c), which shows that the single-layer DL's  $\eta_{\text{PIDE}}^{\text{foc}}$  is around 15 percentage points (p. p.) below the theoretical limit at small values of

$\text{NA}^{\text{dif}}$ . It is evident from figure 7(c) that this leads to a drop of the MTF by at least 10 p.p. for all spatial frequencies. This drop shows that the system's contrast is severely impaired. We note that current metalens designs have even lower polychromatic efficiencies than the single-layer DL [13]. This makes these devices unsuitable for high-quality imaging applications. Finally, to demonstrate the benefits of DLs for broadband imaging systems, we also designed a purely refractive telephoto system with the same specifications as the hybrid system in figure 7. To ensure the comparability of the two systems, we replaced the DL by an additional refractive lens. Furthermore, we kept the constraint that the last two lenses (the second group) must be composed of the same materials as the first two lenses. But we reoptimized the remaining three materials freely using a global optimization scheme. Figure 8(a) presents the layout of the refractive benchmark system. Furthermore, figures 8(b) and (c) depict the refractive benchmark system's focal shift and its MTF, respectively. Both plots show that the purely refractive system's performance is significantly lower than that of the hybrid system (figure 7). Specifically, it is evident from figure 8(b) that the refractive benchmark system is only achromatized ( $f(\lambda_F) = f(\lambda_C)$ ) and not apochromatized ( $f(\lambda_g) = f(\lambda_F) = f(\lambda_C)$ ) like the hybrid system. In fact, we tried forcing the purely refractive system into an apochromatic state but doing so reduced its MTF even further. Comparing the two systems' MTF curves in figures 7(c) and 8(c) shows that the MTF of the purely refractive system is generally around 20 p. p. lower than that of the hybrid system. This demonstrates that integrating a DL into the prototype telephoto system allows for a much higher performance than using the same number of refractive elements. Alternatively, such a performance benefit could generally be leveraged into a size reduction, if the two systems were required to have the same performance. This indicates that integrating DLs into broadband imaging systems indeed holds a high potential for increasing their performance, or alternatively, reducing their size. However, evaluating the full potential of this approach requires systematic optical design studies for a wide range of different systems. In fact, the finding that DLs in broadband systems must only provide little refractive power also implies that that DLs in such systems generally cannot contribute significantly to the correction of monochromatic aberrations. Therefore, our results from section 4 indicate that the highest benefits of DLs can be expected in systems suffering strongly from chromatic aberrations.

In conclusion, the results for the hybrid prototype system confirm that high-NA DLs are not required for broadband systems. In fact, equation (16) predicts a minimum grating period of  $\Lambda_{\min}^{\text{apo}} = 362 \mu\text{m}$  for an apochromat that is composed of the same materials as the hybrid system (N-LAK21 and N-LASF9 with  $q_{\text{apo}} = 54.9$ ). The finding that this value deviates by approximately 40% from the value of  $\Lambda_{\min}^{\text{tele}} = 219 \mu\text{m}$ , which we obtained for the full prototype telephoto system, can be readily understood from the fact that the DL in the telephoto system must work against the dispersion of both lens groups to achieve apochromatization. This demonstrates that, in more complex apochromatic optical systems, the minimum grating period ( $\Lambda_{\min}$ ) might be slightly smaller ( $\text{NA}^{\text{dif}}$  slightly larger)

than the values predicted by equation (16). However,  $\Lambda_{\min}$  will generally be in the same order of magnitude because otherwise the color errors would be highly overcorrected. Therefore, the equations derived in the previous sections can provide a good estimate even for more complex optical systems.

## 6. Conclusion

It has been shown many times that integrating diffractive lenses (DLs) into optical imaging systems often significantly decrease their size or increase their performance [1–8]. For broadband hybrid systems, this is mostly because the anomalous dispersion properties of DLs are perfectly suited for the correction of chromatic aberrations. Conversely, a wide range of different technologies for diffractive optical elements (DOEs), e.g. metalenses and multilevel DOEs [4, 9–22, 26], have been developed. However, often the requirements of optical systems have not been fully taken into consideration. In this paper, we have reconciled these two aspects and analyzed the requirements on DLs both from the optical design as well as the DOE design perspective. To do so, we have derived analytical relationships for achromatic and apochromatic hybrid systems that connect the overall system's specifications (numerical aperture (NA) and focal length) to the parameters of the DL ( $\text{NA}^{\text{dif}} = R/f$  and segment widths). This has allowed us to quantitatively show that DLs with high values of  $\text{NA}^{\text{dif}}$  are not required for broadband systems. In fact, high-NA DLs even impede the performance of such systems since they lead to highly overcorrected chromatic aberrations. Furthermore, we have shown that the minimum segment widths required from DLs in broadband systems are at least in the order of several tens and can even reach hundreds of micrometers. Therefore, the main requirement for the integration of DLs into broadband imaging systems is that the DLs must maintain high focusing efficiencies across the full parameter range required for the system at hand. For example, to achieve a contrast of 1/100 regarding stray light, which is a common requirement for high-end imaging systems, an average efficiency of 99.0% is required.

Finally, we have shown throughout this paper that nanocomposite-enabled DLs fulfill all requirements of high-end broadband systems: They can maintain essentially perfect broadband focusing up to values of  $\text{NA}^{\text{dif}}$  that enable the realization of apochromatic hybrid systems with NAs of up to 1.77 (for common material choices) without any adverse effects on the systems' performance. Furthermore, we have shown that, depending on the value of  $\text{NA}^{\text{dif}}$ , nanocomposite-enabled DLs maintain high efficiencies for a range of angles of incidence of up to 80° (full diagonal). We have discussed and shown on the example of a prototype telephoto lens that this range fully covers the demands of a wide range of systems (e.g. standard and telephoto camera lenses as well as microscopes), whereas the state-of-the-art solutions [4, 9, 45, 46] cannot fulfill these requirements and would drastically impede the systems' performance or lead to severe constraints on the designs. For the first time, we have therefore shown using a holistic all-system analysis that it is indeed possible to unlock the full potential

of DOEs for most broadband optical systems. This guides the way to a next generation of broadband optical systems.

## Funding

This project has received funding from the European Union's Horizon 2020 research and innovation programme under the Marie Skłodowska-Curie (Grant No. 675745). Isabelle Staude gratefully acknowledges the financial support by the Thuringian State Government within its ProExcellence initiative (ACP<sup>2020</sup>) and by the German Research Foundation (STA 1426/2-1).

## Disclosures

The authors declare no conflicts of interest.

## ORCID iDs

Daniel Werdehausen  <https://orcid.org/0000-0002-1559-0811>

Isabelle Staude  <https://orcid.org/0000-0001-8021-572X>

## References

- [1] Greisukh G I, Ezhov E G, Kalashnikov A V and Stepanov S A 2012 Diffractive-refractive correction units for plastic compact zoom lenses *Appl. Opt.* **51** 4597–604
- [2] Stone T and George N 1988 Hybrid diffractive-refractive lenses and achromats *Appl. Opt.* **27** 2960–71
- [3] Greisukh G I, Ezhov E G and Stepanov S A 2006 Diffractive-refractive hybrid corrector for achro- and apochromatic corrections of optical systems *Appl. Opt.* **45** 6137
- [4] Nakai T and Ogawa H 2002 Research on multi-layer diffractive optical elements and their application to camera lenses *Diffractive Optics and Micro-Optics* (Washington, DC: Optical Society of America) p DMA2
- [5] Davison J A and Simpson M J 2006 History and development of the apodized diffractive intraocular lens *J. Cataract. Refract. Surg.* **32** 849–58
- [6] Kazemi A A, Kress B, Starner T, Kress B C and Thibault S 2013 A review of head-mounted displays (HMD) technologies and applications for consumer electronics *Proc. SPIE* **8720** 87200A
- [7] Greisukh G I, Ezhov E G, Levin I A and Stepanov S A 2010 Design of achromatic and apochromatic plastic micro-objectives *Appl. Opt.* **49** 4379–84
- [8] Thiele S, Pruss C, Herkommer A M and Giessen H 2019 3D printed stacked diffractive microlenses *Opt. Express* **27** 35621
- [9] Kleemann B H, Seesselberg M and Ruoff J 2008 Design concepts for broadband high-efficiency DOEs *J. Eur. Opt. Soc.: Rapid Publ.* **3** 08015
- [10] Palmer C A and Loewen E G 2005 *Diffraction Grating Handbook* (New York: Newport Corporation)
- [11] Noponen E, Turunen J and Vasara A 1992 Parametric optimization of multilevel diffractive optical elements by electromagnetic theory *Appl. Opt.* **31** 5910–12
- [12] Kim G, Dominguez-Caballero J A and Menon R 2012 Design and analysis of multi-wavelength diffractive optics *Opt. Express* **20** 2814–23

- [13] Banerji S, Meem M, Majumder A, Vasquez F G, Sensale-Rodriguez B and Menon R 2019 Imaging with flat optics: metalenses or diffractive lenses? *Optica* **6** 805
- [14] Mohammad N, Meem M, Wan X and Menon R 2017 Full-color, large area, transmissive holograms enabled by multi-level diffractive optics *Sci. Rep.* **7** 5789
- [15] Sweatt W C 1977 Describing holographic optical elements as lenses *J. Opt. Soc. Am.* **67** 803
- [16] Decker M, Chen W T, Nobis T, Zhu A Y, Khorasaninejad M, Bharwani Z, Capasso F and Pertsch T 2019 Imaging performance of polarization-insensitive metalenses *ACS Photonics* **6** 1493
- [17] Khorasaninejad M, Zhu A Y, Roques-Carmes C, Chen W T, Oh J, Mishra I, Devlin R C and Capasso F 2016 Polarization-insensitive metalenses at visible wavelengths *Nano Lett.* **16** 7229–34
- [18] Genevet P, Capasso F, Aieta F, Khorasaninejad M and Devlin R 2017 Recent advances in planar optics: from plasmonic to dielectric metasurfaces *Optica* **4** 139
- [19] Decker M, Staude I, Falkner M, Dominguez J, Neshev D N, Brener I, Pertsch T and Kivshar Y S 2015 High-efficiency dielectric Huygens' surfaces *Adv. Opt. Mater.* **3** 813–20
- [20] Lalanne P and Chavel P 2017 Metalenses at visible wavelengths: past, present, perspectives *Laser Photon Rev.* **11** 1600295
- [21] Lalanne P, Astilean S, Chavel P, Cambriil E and Launois H 1998 Blazed binary subwavelength gratings with efficiencies larger than those of conventional échelette gratings *Opt. Lett.* **23** 1081
- [22] Lee M-S L, Lalanne P, Rodier J-C and Cambriil E 2000 Wide-field-angle behavior of blazed-binary gratings in the resonance domain *Opt. Lett.* **25** 1690
- [23] Yu N, Genevet P, Kats M A, Aieta F, Tetienne J P, Capasso F and Gaburro Z 2011 Light propagation with phase discontinuities: generalized laws of reflection and refraction *Science* **334** 333–7
- [24] Larouche S and Smith D R 2012 Reconciliation of generalized refraction with diffraction theory *Opt. Lett.* **37** 2391–3
- [25] Liang H, Martins A, Borges B-H V, Zhou J, Martins E R, Li J and Krauss T F 2019 High performance metalenses: numerical aperture, aberrations, chromaticity, and trade-offs *Optica* **6** 1461–70
- [26] Werdehausen D, Burger S, Staude I, Pertsch T and Decker M 2019 Dispersion-engineered nanocomposites enable achromatic diffractive optical elements *Optica* **6** 1031
- [27] Londono C and Clark P P 1992 Modeling diffraction efficiency effects when designing hybrid diffractive lens systems *Appl. Opt.* **31** 2248–52
- [28] Buralli D A and Morris G M 1992 Effects of diffraction efficiency on the modulation transfer function of diffractive lenses *Appl. Opt.* **31** 4389–96
- [29] Schmidt S, Thiele S, Herkommer A, Tunnermann A and Gross H 2017 Rotationally symmetric formulation of the wave propagation method-application to the straylight analysis of diffractive lenses *Opt. Lett.* **42** 1612–5
- [30] Werdehausen D, Staude I, Burger S, Pertsch T, Scharf T, Pertsch T and Decker M 2018 Design rules for customizable optical materials based on nanocomposites *Opt. Mater. Express* **8** 3456
- [31] Werdehausen D, Scharf T, Pertsch T, Burger S, Pertsch T, Staude I and Decker M 2018 Using effective medium theories to design tailored nanocomposite materials for optical systems *Proc. SPIE* **10745** 107450H
- [32] Werdehausen D, Burger S, Staude I, Pertsch T and Decker M 2019 Nanocomposites—a route to better and smaller optical elements? *Optical Design and Fabrication 2019 (Freeform, OFT)* (Washington, DC: Optical Society of America) p OT2A.2
- [33] Werdehausen D, Burger S, Staude I, Pertsch T and Decker M 2020 General design formalism for highly efficient flat optics for broadband applications *Opt. Express* **28** 6452
- [34] Werdehausen D and Decker M 2020 Diffraktives optisches Element, Verfahren zum Entwerfen einer effizienzachromatisierten diffraktiven Struktur und Verfahren zur Herstellung eines effizienzachromatisierten diffraktiven Elementes *German Patent Application* DE102019109944.7
- [35] Gross H, Singer W, Totzeck M, Blechinger F and Achtner B 2005 *Handbook of Optical Systems* (Weinheim: Wiley) (<https://doi.org/10.1002/9783527699223>)
- [36] Small A 2018 Spherical aberration, coma, and the Abbe sine condition for physicists who don't design lenses *Am. J. Phys.* **86** 487–94
- [37] Schott A G Optical Glass 2018 ([https://www.schott.com/d/advanced\\_optics/c36214d9-13c4-468c-bf40-8d438b89f532/1.14/schott-optical-glass-pocket-catalog-jan-2018-row.pdf](https://www.schott.com/d/advanced_optics/c36214d9-13c4-468c-bf40-8d438b89f532/1.14/schott-optical-glass-pocket-catalog-jan-2018-row.pdf))
- [38] Sultanova N, Kasarova S and Nikolov I 2009 Dispersion properties of optical polymers *Acta Phys. Pol. A* **116** 585
- [39] Chen W T, Zhu A Y, Sanjeev V, Khorasaninejad M, Shi Z, Lee E and Capasso F 2018 A broadband achromatic metalens for focusing and imaging in the visible *Nat. Nanotechnol.* **13** 220–6
- [40] Chen W T, Zhu A Y, Sisler J, Huang Y W, Yousef K M A, Lee E, Qiu C W and Capasso F 2018 Broadband achromatic metasurface-refractive optics *Nano Lett.* **18** 7801–8
- [41] Wang S et al 2018 A broadband achromatic metalens in the visible *Nat. Nanotechnol.* **13** 227–32
- [42] Wang P, Mohammad N and Menon R 2016 Chromatic-aberration-corrected diffractive lenses for ultra-broadband focusing *Sci. Rep.* **6** 21545
- [43] Swanson G J 1989 *Binary Optics Technology: The Theory and Design of Multi-level Diffractive Optical Elements* (Lexington, MA: Lincoln Laboratory Massachusetts Institute of Technology)
- [44] Sandfuchs O, Brunner R, Pätz D, Sinzinger S and Ruoff J 2006 Rigorous analysis of shadowing effects in blazed transmission gratings *Opt. Lett.* **31** 3638
- [45] Glass A J, Weible K J, Schilling A, Herzig H P, Lobb D R, Goodman J W, Chang M, Guenther A H and Asakura T 1999 Achromatization of the diffraction efficiency of diffractive optical elements *Proc. SPIE* **3749** 378–9
- [46] Seesselberg M, Ruoff J and Kleemann B H 2007 Diffractive optical element for colour sensor has multiple successive curvatures structure at right angles to extension direction *German Patent Application* DE102006007432
- [47] Kingslake R 1963 *Lenses in Photography: The Practical Guide to Optics for Photographers* (New York: Garden City Books)
- [48] Hartmann P, Jedamzik R, Reichel S and Schreder B 2010 Optical glass and glass ceramic historical aspects and recent developments: a Schott view *Appl. Opt.* **49** D157–6
- [49] Hartmann P 2015 Optical glass: deviation of relative partial dispersion from the normal line—need for a common definition *Opt. Eng.* **54** 105112